Structure and Size of Bimetallic Palladium-Platinum Clusters in an Hydrotreatment

D. Bazin, D. Guillaume, Ch. Pichon, D. Uzio, S. Lopez

▶ **To cite this version:**

D o s s i e r

Synchrotron and Neutron Solutions to Oil Industry Problems
Utilisation des grands instruments analytiques dans l'industrie pétrolière

Structure and Size of Bimetallic Palladium – Platinum Clusters in an Hydrotreatment Catalyst

D. Bazin[1], D. Guillaume[2], Ch. Pichon[3], D. Uzio[2] and S. Lopez[2]

1 LPS, Université Paris XI, Bât. 510, 91898, Orsay - France
2 IFP Lyon, Catalysis & Separation Division, BP3 69390 Vernaison - France
3 IFP Lyon, Physics and Analysis Division, BP3 69390 Vernaison - France
e-mail: bazin@lps.u-psud.fr - denisjm.guillaume@ifp.fr - christophe.pichon@ifp.fr - denis.uzio@ifp.fr - sylvie.lopez@ifp.fr

Résumé — Structure et taille de particules bimétalliques palladium – platine dans un catalyseur d'hydrotraitement — Des catalyseurs bimétalliques PdPt supportés sur alumine ont été synthétisés par imprégnation à sec de bis acétylacétonate. Les formulations Pt_4Pd/Al_2O_3 and Pt_6Pd/Al_2O_3 dédiées à l'hydrogénation des aromatiques et à la désulfuration, ont été caractérisées par spectroscopie d'absorption X, microscopie électronique à transmission, et titrage H_2-O_2. Il a été montré que les métaux étaient associés dans des structures de type cœur-coquille avec un enrichissement préférentiel de la surface des particules en Pd. De plus, la composition optimale pour la réaction d'hydrogénation des aromatiques en présence de soufre est dépendante de la taille des particules.

Abstract — Structure and Size of Bimetallic Palladium – Platinum Clusters in an Hydrotreatment Catalyst — Highly dispersed supported bimetallic PdPt catalysts were prepared by incipient wetness co-impregnation of alumina with platinum bis-acetylacetonate $Pt(Acac)_2$ and palladium bis-acetylacetonate $Pd(Acac)_2$. The resulting Pt_4Pd/Al_2O_3 and Pt_6Pd/Al_2O_3 catalytic systems dedicated to hydro-dearomatization in presence of sulfur were characterized by X-ray absorption spectroscopy, transmission electron microscopy and volumetric H_2-O_2 titration. Direct structural evidence is given of the presence of nanometer bimetallic particles. Moreover, the complete set of results indicates a "cherry-like" structure for the bimetallic clusters with a preferential distribution of palladium atoms at the cluster surface. Catalytic results shows that the optimum composition leading to the appropriate surface structure must be adjusted as a function of the size of the clusters.

INTRODUCTION

In both Europe and the United States of America, legislation is imposing more and more stringent reduction of the aromatic hydrocarbons contained in car diesel fuels [1]. In addition to their carcinogenic characteristic, mono- or poly-cyclic aromatics lower the diesel fuel quality by lowering the cetane index [2]. To remove these undesirable compounds, a catalytic hydroconversion, on transition metal (mainly platinum), is generally suggested.

One of the main difficulties is the presence of sulfur in the feedstock, which is still too high, even if hydro-desulphurization treatments have achieved great progress, to use a standard hydrogenation noble metal catalyst. Because, even at such a low concentration, sulphur rapidly deactivates the de-aromatizing catalyst, a thio-tolerance of the catalyst is required [3]. Various catalytic systems have already been investigated in the literature combining a thio-tolerant metallic phase with supports with different acido-basic surface properties [4-8], with addition of promoters [9-10] or alloying the Pt base catalyst with other metallic elements [11-12].

Many patents and articles claim that PdPt supported bimetallic catalysts are more thio-tolerant than pure metals [13] particularly for a selected range of Pd/Pt ratio [14-17]. Regarding academic studies, several studies have been already dedicated to the structure at the atomic scale of this bimetallic catalyst [18-22]. In some cases, contradictory results were found with no enhancement of the sulfur resistance or hydrogenation activity [23-24].

Interpretations proposed in the literature suggest that the modification of the sulphur sensitivity could be related to strong interactions between the two metals organized in core-shell structured particles. Structural and electronic characteristics depend intimately on the preparation procedure itself [25] and on the different parameters of the procedure such as the calcination temperature [26-28].

We report here a study of highly dispersed Pt-Pd catalytic systems deposited on cubic γ-alumina with different Pd/Pt atomic ratios. We have concentrated our attention on the metallic function of the catalysts. Thus, we have combined different techniques, namely X-ray absorption spectroscopy [29], TEM (Transmission Electron Microscopy) and volumetric H_2-O_2 titration. The ultimate goal of this structural and electronic investigation at the atomic scale is to give clear structural evidence of the presence (or not) of heterometallic bonds inside the catalyst. Moreover, the complete set of results allows us to propose a model regarding the distribution of the two metals inside the bimetallic particles.

2 EXPERIMENTAL

2.1 Catalyst Preparation

The catalysts are highly dispersed Pt, Pd monometallic and bimetallic Pt-Pd system deposited on alumina extrudates. More precisely, the support used was a cubic γ-alumina with a specific area of 280 m²/g (+/- 10 m²/g) and a pore volume of 0.7 cm³/g. Two compositions were chosen with different metal loadings corresponding to atomic Pd/Pt ratios of 4 and 6.

Pd-Pt/Al_2O_3 catalysts were prepared by incipient wetness co-impregnation of alumina with platinum bis-acetylacetonate Pt(acac)$_2$ and palladium bis-acetylacetonate Pd(acac)$_2$ according to the procedure described for example in references [30-31]. The two complexes were dissolved in toluene and the organic solution put in contact with alumina during 72 h at room temperature. After activation under airflow at 350°C during 2 h, the catalyst was reduced 2h at 450°C under nitrogen flow.

0.6% wt Pt and 0.4% wt Pd monometallic catalysts were also prepared using the same support and procedure in order to have reference catalysts.
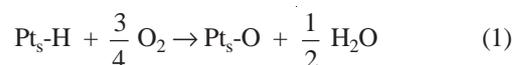
2.2 Transmission Electron Microscopy (TEM)

TEM was carried out on a JEOL-2010 at 200 kV. After grinding in an agate mortar and sieving, the catalyst was suspended in ethanol and the suspension was then deposited on a copper grid covered with a carbon membrane. During the measurement, the sample was maintained under secondary vacuum. Histograms were constructed from the observation of around 300 particles.
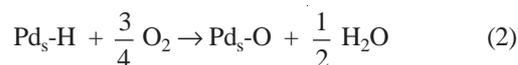
2.3 Volumetric hydrogen - oxygen titration

The titration of adsorbed H_2 by O_2 has been used to determine the metallic dispersion and average particle size with a χ-sorb® apparatus. The catalysts were reduced before the titration by oxygen of the hydrogen chemisorbed on the accessible metal atoms. The reduction was performed under pure H_2 flow for 2 hours at 300°C with a intermediate stage of 1 hour at 150°C. After reduction, the catalyst was cooled under hydrogen flow and the sample cell was purged at 25°C under N_2 flow. Pulses of O_2 were repeatedly injected into the catalyst bed until no further consumption of O_2 was observed. The total volume of O_2 was then calculated by summing up the proportions of all pulses consumed. The relative accuracy of the measurement is 5%.

The titration follows equations (1) and (2):

$$Pt_s\text{-}H + \frac{3}{4} O_2 \rightarrow Pt_s\text{-}O + \frac{1}{2} H_2O \qquad (1)$$

and

$$Pd_s\text{-}H + \frac{3}{4} O_2 \rightarrow Pd_s\text{-}O + \frac{1}{2} H_2O \qquad (2)$$

The dispersions D of the monometallic and bimetallic particles are determined according to equations (3) and (4):

$$D\,(\%) = \frac{V\,n\,M}{V_m\ \%\text{wt}} \qquad (3)$$

$$D\ (\%) = \frac{V\ n\ M_{Pd}\ M_{Pt}}{V_m\ (\%Pt * M_{Pd} + \%Pd * M_{Pt})} \quad (4)$$

Mean particle size is obtained via the relations proposed by Van Hardeveld and Hartog [32] for regular truncated cubo octahedron geometry:

$$N_t = 16\ m^3 - 33\ m^2 + 24\ m - 6 \quad (5)$$

and

$$N_s = 30\ m^2 - 60\ m + 32 \quad (6)$$

with:

m order of the cubo octahedron ($m \geq 2$).
N_t total number of atoms
N_s number of surface atoms

Dispersion defined by the ratio $D = \dfrac{N_s}{N_t}$ allows one to calculate successively m, N_t and the diameter d of a sphere containing N_t atoms given by:

$$d = \frac{2(3N_tV_a)^{1/3}}{(4\pi)^{1/3}} \quad (7)$$

Metallic surface area S (m^2/g $_{catalyst}$) is obtained using the relation:

$$S = \frac{VnN}{\sigma V_M} \quad (8)$$

with:

V_a atomic volume (8.9 cc/mol mean value for Pd and Pt) [33].
σ number of atoms per m^2 (1.27×10^{19} atoms/m^2)
N Avogadro number
n stoichiometry metal / adsorbate
V_M molar volume of adsorbate at T (22400 cm^3/g)
M molecular weight (g.mol^{-1})
V adsorbated volume (cc/g catalyst).

Note that this semi - empirical formula gives mean diameter values very close to those calculated with more realistic models as proposed in reference [23].

2.4 Electron Micro Probe Analysis

For EMPA (Electron Micro Probe Analysis) characterization, sample extrudates were embedded in a metacrylate resin, polished with SiC paper and coated with carbon black. Measurements were performed with a JEOL JXA 8800R microprobe fitted with four WDS spectrometers. Electron beam conditions were 20 kV accelerating voltage, 40 nA beam current and a focused probe. The Al Kα, Pt Mα and Pd Lα lines were acquired using respectively TAP, PETH and PETH crystals. Counting times on both peak and background

were respectively 10, 20 and 20 s. Elemental quantification was performed using a ZAF procedure, oxygen being calculated by stoichiometry (Al$_2$O$_3$). About 24 analysis points were acquired every 50 µm along the diameter on five different sample extrudates.

2.5 Extended X-ray Absorption Fine Structure (EXAFS)

X-ray absorption experiments (with both *in situ* and *ex situ* reduced catalysts) were performed at the LURE laboratory using DCI, a storage ring operated with an electron energy of 1.85 GeV and a current between 260 and 360 mA. Data were collected on the EXAFS IV station, a beam line placed after a bending magnet which is equipped with a double crystal monochromator, Si(111) for the Pt L$_{III}$-edge (11564 eV) and Si(311) for the Pd K-edge (24352 eV), and a double borosilicate mirror for the rejection of harmonics. Measurements were done either in transmission mode (using ionisation chambers filled with air to absorb around 20% of the X-ray beam in the first ion chamber and the remainder of the X-ray beam in the second ion chamber) or in fluorescence mode using a multi-detector element. More precisely, transmission mode was used to perform experiments at the Pd K-edge whereas fluorescence mode was used at the Pt L$_{III}$-edge. Only the Pd$_6$Pt catalyst was studied by EXAFS spectroscopy.

At the Pd K-edge, the spectrum was recorded twice with a step of 4 eV (from 24150 to 25350 eV) and 2 s per point. At the Pt L$_{III}$-edge, each spectrum was recorded twice with a step of 2 eV (from 11450 to 12450 eV) and 5 s per point. At the Pd K-edge, as well as the Pt L$_{III}$-edge, the estimated energy resolution of the monochromator was approximately 3 eV. The energy/angle calibration was performed using either a Pd foil (thickness 7.5 µm) or a Pt foil (thickness 7.5 µm) as references. After sieving, particles in the 100-200 µm range were either loaded into a sample holder sealed by self-adhesive tape made of Capton$^®$ for experiments in transmission mode (Pd K-edge) or agglomerated and loaded into a sample holder (Pt L$_{III}$-edge).

The Pd K-edge was recorded at room temperature under atmospheric pressure. Regarding the experiments in fluorescence mode, the sample was placed in a special furnace for *in situ* treatment with entrance and exit windows made of boron nitride that is transparent to the X-ray beam [34-35].

The *in situ* reduction of the catalyst was performed at 350°C, under pure hydrogen, during 1 hour. The Pt L$_{III}$-edge was recorded at room temperature under 1 bar pressure of pure nitrogen. Note that *in situ* reduction of the catalyst was followed by XANES (X-ray Absorption Near Edge Structure) measurements. Normalized EXAFS spectra were isolated from the experimental data using a standard procedure [36-37].

Fourier transforms (FT) of the k^3 weighted EXAFS functions were obtained using a Kaiser type window ranging between 3.35 and 13.00 Å^{-1} beyond the Pd K-edge and

between 2.04 and 8.80 Å^{-1} beyond the Pt L$_{III}$-edge (the spectra are noisy above those limits). In this work, all FT are calculated and presented without phase correction. The inverse FT were obtained in the range between 0.169 and 0.318 nm for palladium and between 0.120 and 0.380 nm for platinum. Palladium and platinum metallic foils were employed as references for the Pt-Pt and Pd-Pd bonds [38], while a metallic alloy PtPd was used for Pd-Pt bonds [39].

Regarding the metal-oxygen bonds, the reference powder PdO was used for the Pd-O bond and the reference powder PtO$_2$ was used for the Pt-O bond. Structural parameters (co-ordination numbers and interatomic distance) of the reference compounds used in this study are summarized in Table 1. A two-shell least-squares fitting procedure (in k-space) using a single scattering EXAFS formulation was used to extract the co-ordination number (N), distance (R) and Debye-Waller factor ($\Delta\sigma$). Figure 1a and 1b show the quality of agreement obtained in k and R space between filtered experimental data and numerical simulation for the Pd K-edge EXAFS spectrum of the Pd-Pt catalyst. Note that the numerical simulation corresponds to a typical residual of the order of 10^{-2}.

TABLE 1

Structural parameters (co-ordination number N, interatomic distance R) of the reference compounds

	Pd foil	Pt foil	Pd-Pt alloy	PdO	PtO$_2$
N	12	12	12	6	6
R (Å)	2.75	2.76	2.73	2.00	2.05

2.6 Catalytic Tests: Hydrogenation of Aromatic Feed with Sulfur Addition

Hydrogenation runs were carried out in a bench scale plant test containing an isothermal fixed bed reactor operating in up-flow mode. Feedstock was a deeply desulfurized Light Cycle Oil (DLCO) which has been prepared by hydrotreating a pure Light Cycle Oil (LCO). LCO is a middle distillate refinery product generated in a fluid catalytic cracking (FCC) unit. The main properties of DLCO are summarized in Table 2. The DLCO has a very low sulfur and a high aromatic content. The sulfur content of this feed has been increased artificially up to 200 ppm S by adding dibenzothiophene (DBT). This procedure allows evaluating the effect of the amount of sulfur on the hydrogenating properties of catalysts for a same aromatic composition of the feed.

Hydrogenation of DLCO feed was carried out under the following conditions: 25 cm^3 of catalysts in 1.2 mm extrudated shape diluted in 25 cm^3 of SiC (in the 1-3 mm particle size range), a total pressure of 6 Mpa, reaction temperature of 300°C, liquid hourly space velocity (LHSV) of 5 h^{-1}, hydrogen-to-feed oil ratio (without recycle) of 450 NL/L.

The catalyst was dried *in situ* under pure H$_2$ flow for 4 h at 150°C before being reduced at 300°C for 2 h. After reduction, the catalyst was cooled to 150°C. The initial DLCO feedstock was introduced and the test conditions were adjusted. The change of feedstock containing different sulfur contents was realized after stabilization of performances. In practice, about 300 hours are necessary to stabilize the catalysts. During this first period, the catalysts are passivated by
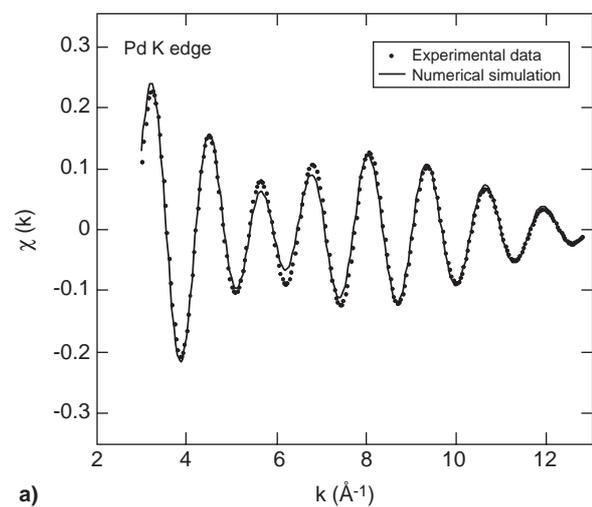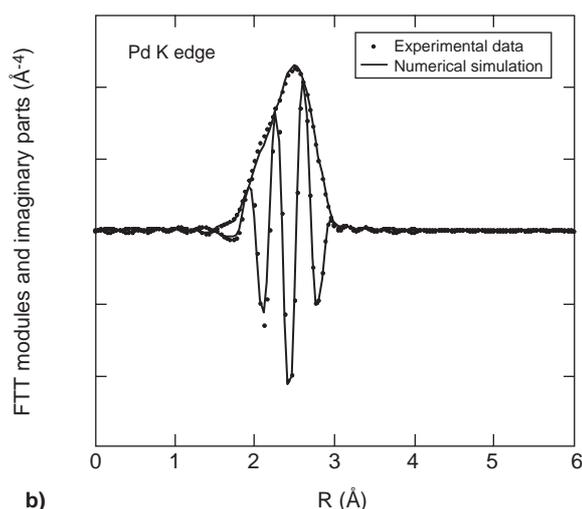

a)

Figure 1a

Quality of numerical simulation of the EXAFS modulations obtained on the k(Å^{-1}) space for Pd$_6$Pt/Al$_2$O$_3$ at the Pd K edge.

b)

Figure 1b

FFT imaginary parts and modulus illustrate the quality of numerical simulations obtained on the R(Å) space for Pd$_6$Pt/Al$_2$O$_3$ at the Pd K-edge.

sulfur. After that passivation, about 100 hours are necessary to stabilize the catalysts when DBT is added to the feedstock.

<div align="center">

TABLE 2

Composition of the feed (DLCO)

</div>

Sulfur, wt ppm	20
Nitrogen, wt ppm	7
Density (15°C), g/cm^3	0.8874
Paraffins, wt% (MS)	16.4
Naphtenes, wt% (MS)	31.4
Total aromatics, wt% (NIR/MS)	52.2
Mono aromatics,wt%	39.9
PAH, wt%	12.3
Distillation, IP/FP, °C	169/393
Cetane Number (NIR)	38

The percentage and type of aromatics (total aromatics, mono-aromatics and poly-aromatics) in the feed and the products were measured by near infrared (NIR) spectroscopy correlated to the Fitzgerald method based on mass spectrometry (MS) measurements. The cetane number was also determined by NIR spectroscopy correlated to ASTM D613 (cetane motor). The NIR spectra were recorded on nitrogen purged Bomem MB160 FT-NIR spectrometers equipped with a DTGS (deuterated tri glycide sulfide) detector, operating in transmission mode with a resolution of 4 cm^{-1}. Total amount of sulfur in the products was measured by X-ray fluorescence.

The decrease in the total aromatics content in DLCO was assumed to be pseudo-first-order. The rate constant was defined by the following equation:

$$k_a \ (h^{-1}) = \ln(C_{feed}/C_{product}) \times LHSV$$

with:
C_{feed} concentration of aromatic in feedstock and
$C_{product}$ concentration of aromatics in product.

3 RESULTS

3.1 Main Characteristics

Table 3 summarizes the main characteristics of the catalysts. Nominal compositions are Pd$_4$Pt and Pd$_6$Pt. Both elements are very homogeneously distributed along the radial dimension of the extrudates as shown by the R coefficient, very close to 1 *(Fig. 2)*. The symmetry of the two profiles is consistent with a close association of the two metals at least at the resolution of the Castaing microprobe analysis (about 1 μm). The dispersions and the mean diameters determined from H$_2$-O$_2$ titration measurements are similar for the two catalysts.

<div align="center">

TABLE 3

Main characteristics of mono and bimetallic catalysts

</div>

Catalysts	Pt	Pd	Pd$_4$Pt	Pd$_6$Pt
Pt wt%	0.6		0.18	0.20
Pd wt%		0.4	0.42	0.67
Pd/Pt molar ratio			4.3	6.1
R (Pt)	0.98		0.96	0.96
R (Pd)		0.97	0.96	1.02
support specific surface area (m^2/g)	265	265	261	292
O$_2$ volume (cc/g$_{catalyst}$)	0.47	0.59	0.57	0.88
Dispersion %[1]	84	85	64	66
Mean Diameter (nm)[2]	1.3	1.3	1.6	1.6
Metallic surface area (m^2/g$_{catalyst}$)[3]	124	151	165	251

1 calculated with equation (3) or (4).
2 calculated with equation (7).
3 calculated with equation (8) and corrected by the % weight of metal.

3.2 Transmission Electron Microscopy (TEM)

Regarding the support, electron microscopy shows that the specimen is dominated by a single morphology. More precisely, the different TEM photographic pictures show small plates of cubic γ-alumina extrudates, of 1-10 nm in length.

A TEM photograph and the particle size distribution of the Pd$_6$Pt catalyst, obtained by a statistical analysis of several micrographs, are presented on Figure 3. Most of the particles have a size around 1 nm and the average size by number is 1.8 nm. Larger particles up to 6 nm are also present but to a much lower extent. The probe size is too large compared to the size of the particles to determine the distribution of the different metal elements of the individual catalyst particles.

3.3 Atomic Structure: EXAFS Measurements

The XANES part of the absorption spectrum for Pd$_6$Pt catalyst is plotted in Figure 4. After *in situ* treatment under H$_2$, the platinum atoms are reduced to metallic state as indicated by the similarity in the intensity of the white line of the Pt foil to that of the catalyst [40-41]. Moreover, a comparison of the EXAFS part of the absorption spectra for Pd$_6$Pt catalyst *(Fig. 5)* clearly indicated that the local environment of Pt atoms essentially consists of metal atoms. This is confirmed by the shape and the position of the FT modulus *(Fig. 6)* as well as by the coordination numbers given by the numerical simulation of the EXAFS oscillations *(Table 4)*. More precisely, quantitative analysis gives 3.4 for the average number of platinum atoms and 6.7 for average number of palladium atoms around platinum atoms.
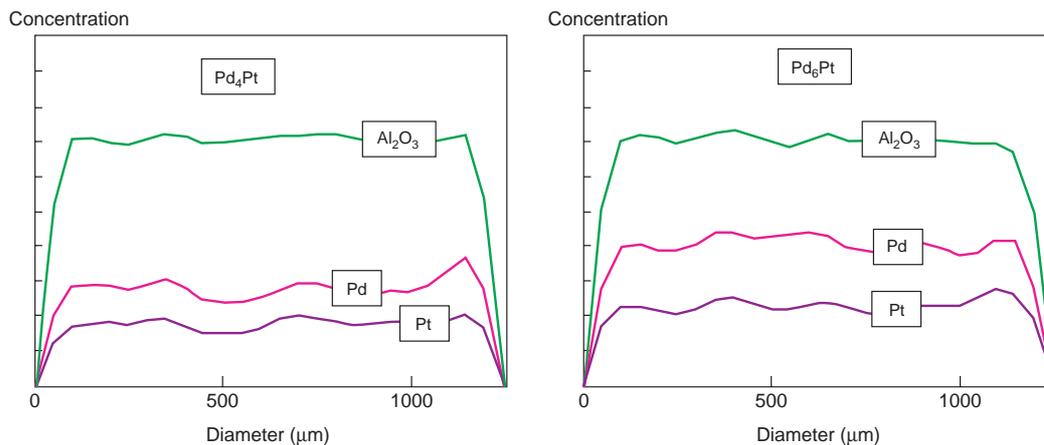
Figure 2

Metallic repartitions of platinum and palladium for both Pd_6Pt/Al_2O_3 and Pd_6Pt/Al_2O_3 catalysts by EPMA.

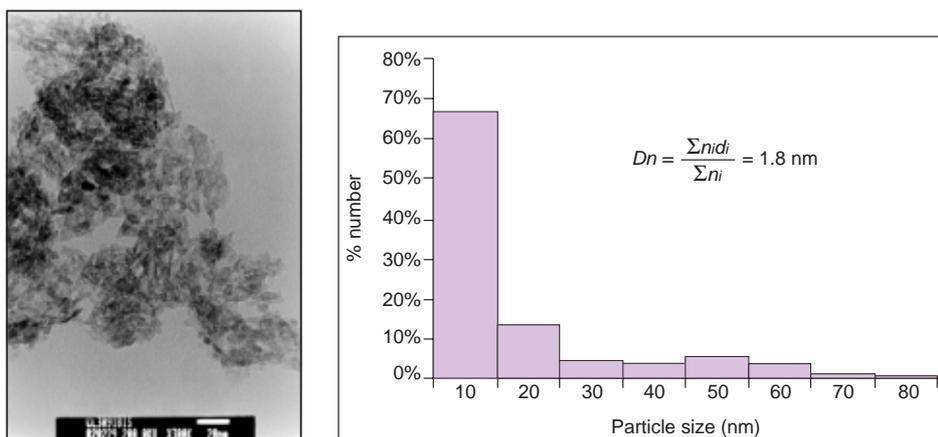Figure 3

TEM micrographs (with large metallic particles) and histogram of the Pd_6Pt catalyst.
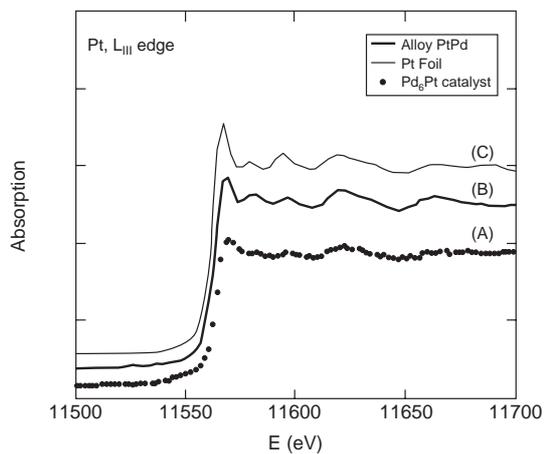

Figure 4

XANES spectra collected at the Pt L_{III} edge for the Pd_6Pt catalyst (A) compared to the alloy PtPd metallic foil (B) and the Pt metallic foil (C).
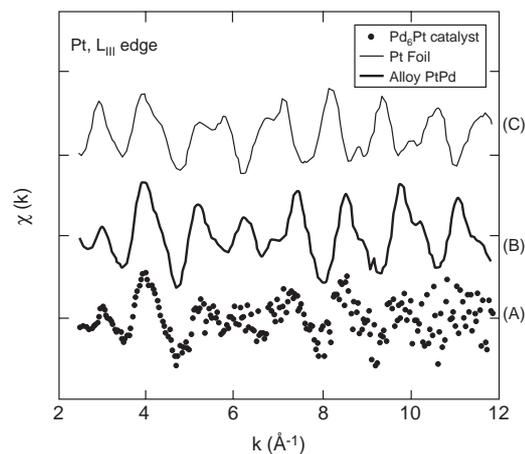

Figure 5

EXAFS data collected at the Pt L_{III} edge for the Pd_6Pt catalyst after *in situ* H_2 reduction (A) compared to the alloy PtPd metallic foil (B) and the Pt metallic foil (C).
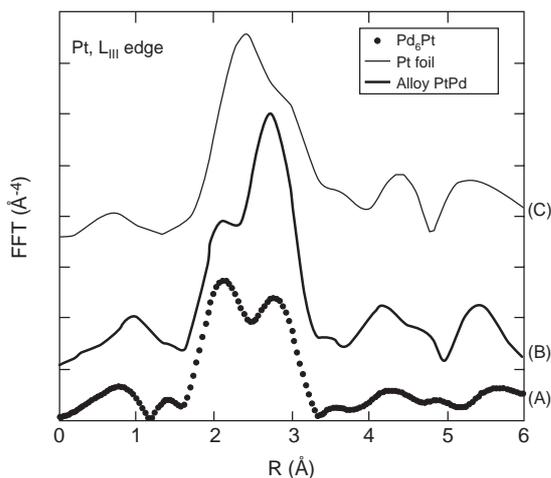
Figure 6

F.T. modules obtained at the Pt L$_{III}$ edge for the Pd$_6$Pt catalyst after the *in situ* reduction (A) compared to the alloy PtPd metallic foil (B) and the Pt metallic foil (C).

Figure 7

XANES spectra collected at the Pd K edge for the Pd$_6$Pt catalyst (A) compared to the alloy PtPd metallic foil (B) and the Pd metallic foil (C).

TABLE 4

Parameters for numerical simulation of EXAFS data at Pd K-edge or Pt L$_{III}$-edge for Pd$_6$Pt catalyst

Edge	Pd K-edge	Pt L$_{III}$-edge
Scale factor	1.00	1.00
Number of shells	2	2
Nature of the shell	Pd	Pt
Number of neighbours (N)	6.9 (± 0.5)	3.4 (± 0.5)
Distance (R)	2.73Å (± 0.05)	2.67Å (± 0.05)
Debye-Waller factor (Δσ)	0.02Å	0.01Å
Edge shift	2.5 eV	–3.2 eV
Nature of the shell	Pt	Pd
Number of neighbours (N)	0.9 (± 0.5)	6.7 (± 0.5)
Distance (R)	2.77Å (± 0.05)	2.82Å (± 0.05)
Debye-Waller factor (Δσ)	0.03Å	0.01Å
Edge shift	2.1 eV	0.0 eV

Figure 8

EXAFS modulations collected after the Pd K edge for the Pd$_6$Pt/Al$_2$O$_3$ catalyst after the *in situ* reduction (A) compared to the Pd metallic foil (B) and the alloy PtPd metallic foil (C).

A similar approach was carried out at the Pd K-edge. The XANES part of the absorption spectra collected at the Pd K-edge after *in situ* reduction of the Pd$_6$Pt/Al$_2$O$_3$ catalyst *(Fig. 7)* indicates clearly that the palladium atoms are reduced to metallic state [42].

Also, a comparison of the different EXAFS parts for Pd$_6$Pt catalyst above the Pd K-edge shows that the local environment of Pd atoms essentially consists of metal atoms *(Fig. 8)*. Finally, FT modules as well as the values of the different coordination numbers, confirmed these observations *(Fig. 9)*. Regarding the metallic particles present inside the bimetallic catalyst, the analysis of the EXAFS modulations present beyond the Pd K-edge shows for the local environment of palladium 6.9 Pd atoms at 0.273 nm and 0.9 Pt atoms at 0.277 nm.
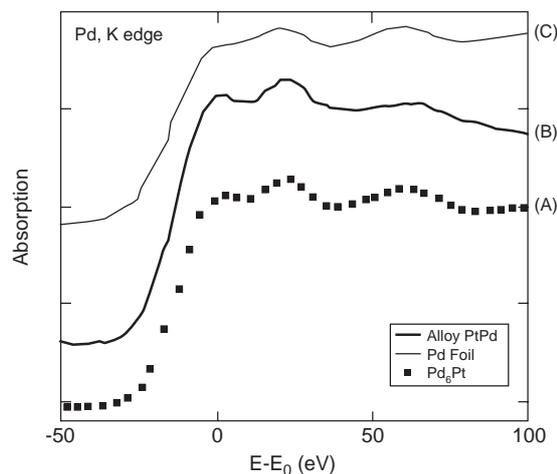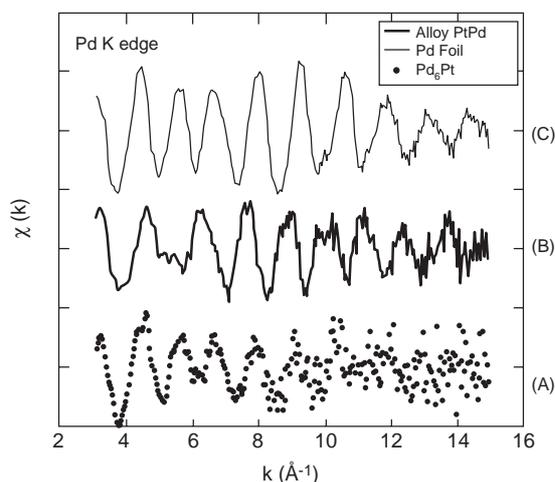
As previously underlined [43], we have in the case of bimetallic clusters, the following relationship:

$$R_{PtPd} = R_{PdPt}, \sigma_{PtPd} = \sigma_{PdPt}, C_{Pt} N_{PtPd} = C_{Pd} N_{PdPt}$$

where C_A and C_B corresponds to the atomic concentration of the two metals.

The different measured bond lengths in the samples gave results in good agreement with those calculated in the experimental references. Pd-Pt bond lengths measured at Pd K-edge and Pt L$_{III}$-edge are not exactly the same but are coherent with the estimated error of the measurement. Pd-Pd bond

length in the catalyst is typical of metallic material. Pt-Pt bond length is a little short but remain acceptable. The equality regarding the Debye-Waller factor is also respected. Finally, the relationship between the coordination numbers N_{PtPd} (average number of palladium atoms around platinum) and N_{PdPt} (average number of platinum atoms around palladium) is respected, the atomic ratio between platinum and palladium being equal to 6.
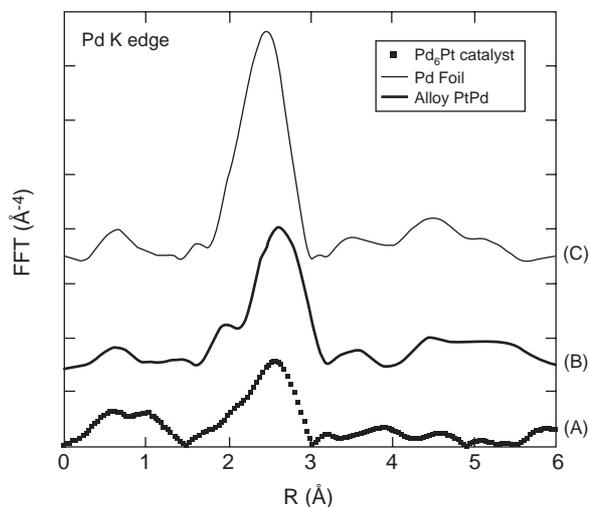

Figure 9

FT modules obtained at the Pd K edge for the Pd_6Pt catalyst after the *in situ* reduction (A) compared to the alloy PtPd metallic foil (B) and the Pd metallic foil (C).

3.4 Catalytic Results: Hydrogenation of Aromatic Feed with Sulfur Addition

The Figure 10 shows that the activity of both bimetallic catalysts decreases when the sulfur content of the feed increases. Nevertheless, for each sulfur content in the feed, the Pd_6Pt catalyst is found more active than the Pd_4Pt catalyst in terms of rate constants. The Figure 11 presents the aromatic contents and the cetane number measured for the products using the Pd_4Pt and Pd_6Pt catalysts. The higher cetane numbers obtained with the Pd_6Pt catalyst are in accordance with its higher efficiency in hydrogenation in presence of sulfur. This appears essentially by a better mono-aromatics saturation, the gain in poly-aromatics saturation being less important. On the other hand, at 20 ppm of sulfur in the feed, the Pd_6Pt catalyst allow to reach a PAH (Poly Aromatic Hydrocarbons) target which is inferior to 2 wt % (in the conditions used) contrary to the Pd_4Pt catalyst for which the PAH content equals 4 wt%.

Besides the aromatic reduction, hydrodesulfurization is also performed. The sulfur content of products versus sulfur content of the feed is presented in Figure 12. We note that the Pd_6Pt catalyst is more efficient in desulfurizing the feed than the Pd_4Pt catalyst when the sulfur content of the feed increases (between 20 and 50 ppm of sulfur in the feed, the conversion differences are negligible, whilst they are significant at higher sulfur content).

4 DISCUSSION

Regarding the size of the metallic particles, the complete set of data, coming from HRTEM, volumetric H_2-O_2 titration
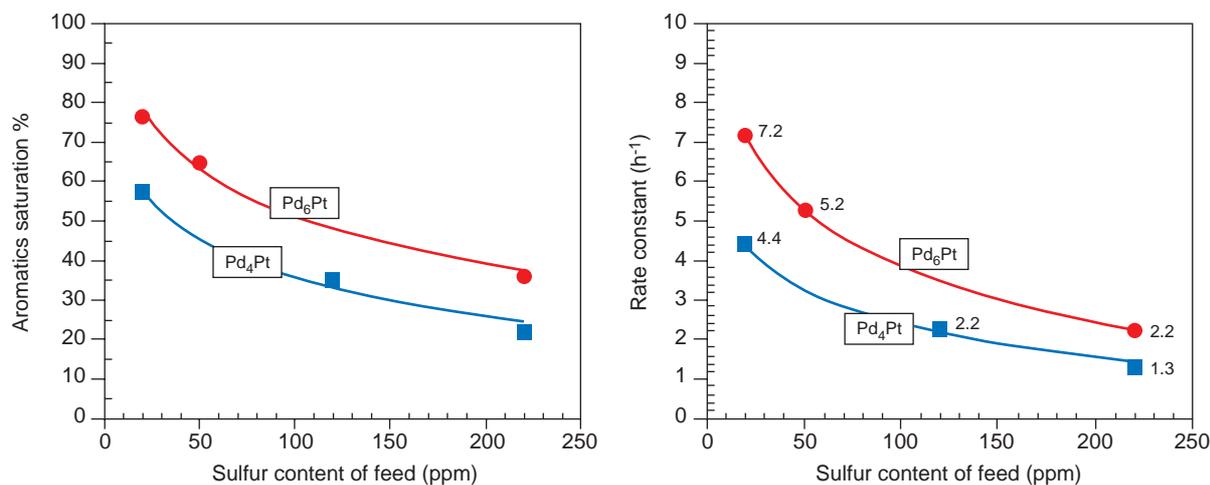

Figure 10

Sulfur resistance of the bimetallic catalysts: Aromatics saturation (%) and rate constant (h^{-1}) versus sulfur content of the feed.
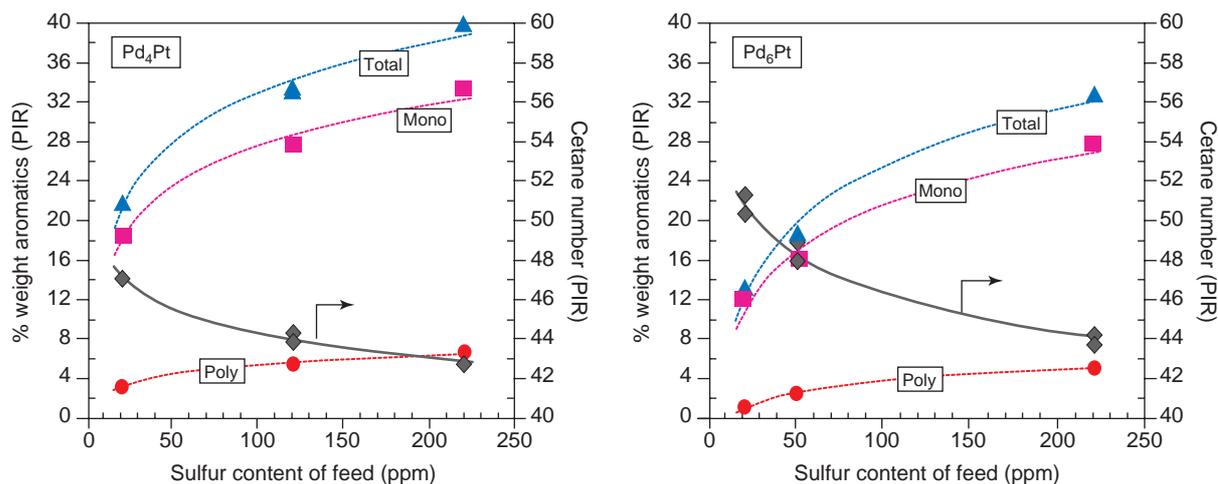
Figure 11

Distribution of aromatics and cetane number for Pd_4Pt and Pd_6Pt catalysts versus the amount of sulfur in the feed.
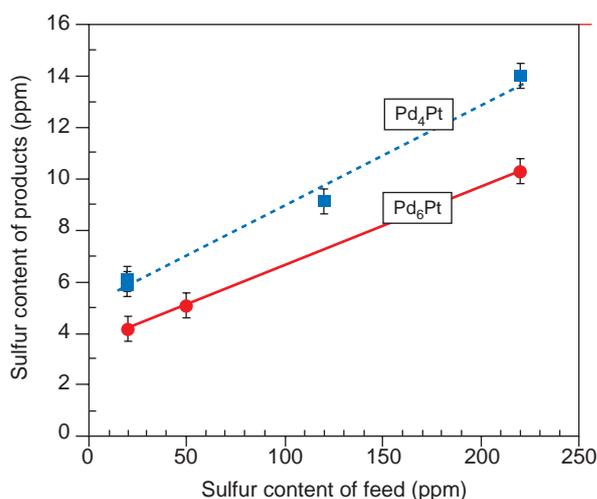

Figure 12

HDS catalytic performances of bimetallic catalysts.

and X-ray absorption spectroscopy, indicate the presence of nanometer scale metallic particles for the Pd_6Pt catalyst. The results given by each technique are quite coherent if we take into account the different advantages and limitations of each characterization technique. Since the limit of detection of TEM is about 6 to 8 Å, very small metallic particles (less than 6 Å in diameter) may exist on the catalyst, which were not detected by TEM. However, whereas the TEM technique can distinguish several populations of metallic particles with different sizes, X ray absorption spectroscopy and volumetric H_2/O_2 titration can only provide an average particle size. The

key point of the EXAFS data is to point out the existence of heteroatomic bonds. At both Pd K-edge and Pt LIII-edge, bonds between palladium and platinum were characterized. Several studies [44-47] have used the synchrotron radiation specific X-ray absorption spectroscopy to give direct structural evidence of the presence or not of bimetallic clusters. The fact that our experiments are performed *in situ* allows us to build a structural model through the structural characteristics at the atomic level obtained with the different techniques. But what is the distribution of the two metals inside the bimetallic particle ?

From a theoretical point of view [48-49] we have now the possibility to describe in a realistic way the electronic structure of nanometer scale metallic clusters and thus to understand both their atomic and chemical rearrangements [50-51]. Moreover, the element with the lowest surface energy is indeed found enriched at the surface: Pd in Pt–Pd and Pt in Pt–Mo, Pt–Rh and Pt–Ru.

From an experimental point of view, the segregation of Pd has been observed in several studies [52]. More recently, nanometer sized particles of platinum and palladium have been prepared through a reaction of platinum and palladium aqueous salts in water-in-oil microemulsions. M. Yashima [53] noticed that the Pt particles are crystalline while the significantly smaller palladium particles are mostly amorphous and often adsorbed on the surface of platinum particles. The presence of palladium at the surface of the nanoparticles has been also pointed out by J. Solla-Gullon [54].

Finally, we have to underline that such distribution between the two metals is not systematic. For example, L. D'Souza [55] found through XPS and CO adsorption studies that the structure of the particles consists of a palladium core and a platinum shell.

In the case of an homogeneous system for which the core of the cluster is composed of N(Pt) atoms Pt and surface is made of N(Pd) atoms Pd, we have the relationship:

$$[N_{PtPt} + N_{PtPd}]_{Pt\ edge} = 12 > [N_{PtPd} + N_{PdPd}]_{Pd\ edge}$$

Where :

N_{PtPt} is the average number of platinum atoms around platinum (Pt edge),

N_{PtPd} s the average number of palladium atoms around platinum (Pt edge),

N_{PdPt} is the average number of platinum atoms around palladium (Pd edge),

N_{PdPd} is the average number of palladium atoms around palladium (Pd edge).

This hypothesis is based on the absence of monometallic clusters. In the present study, the total number of bonds engaged by the metallic element is more important for platinum *i.e.* N_{PtPt} (= 3.4) + N_{PtPd} (= 6.7) = 10.1 than for palladium *i.e.* N_{PdPt} (= 0.9) + N_{PdPd} (= 6.9) = 7.8. This suggests that the particles have a "cherry" structure: a shell of palladium surrounds a core of platinum atoms.

This approach is consistent with TEM analysis where it appeared that the specimen is dominated by a single morphology of particles. Thus, simple calculations of coordination numbers corresponding of spherical bimetallic particles of different sizes have been considered. In Figure 13, we have selected the case where a shell of palladium atoms surrounds a core of platinum atoms, the core size being considered as a parameter. A simple observation of this figure shows that an agreement can been found between the experimental results and the set of these simple calculations. In order to evaluate the uncertainty for the composition of the surface of the metallic cluster, we have chosen another family of clusters. In Figure 14, the core of platinum atoms contains 13 atoms and the number of shells of palladium atoms is considered as a parameter. Due to the size distribution, it is quite clear that the composition of the surface cannot be precisely determined in terms of the number of surface shells of palladium atoms. But it remains that, in the majority, the particles were found bimetallic, with a "cherry" structure with a preferential distribution of palladium atoms at the cluster surface.

TEM or EXAFS experiments were not performed on the Pd_4Pt catalyst. But since we used the same preparation techniques for the two catalysts and since the results of H_2-O_2 volumetric titration were very comparable, the particle size for the two catalysts will be assumed to be the same.

Figure 13
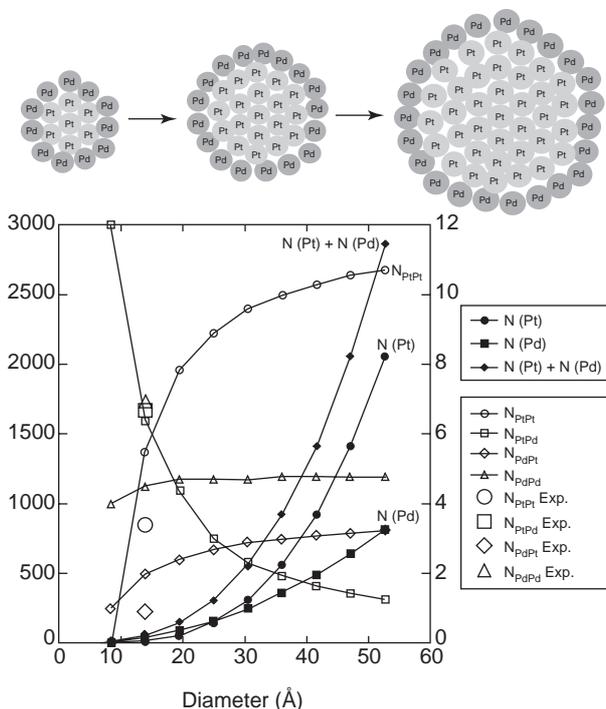
Coordination numbers N_{PtPt}, N_{PtPd}, N_{PdPt} , N_{PdPd} (the core of the cluster is composed of N(Pt) atoms Pt and surface is made of N(Pd) atoms Pd, the size of the core of platinum atoms is considered as a parameter) compared to experimental values.

Figure 14
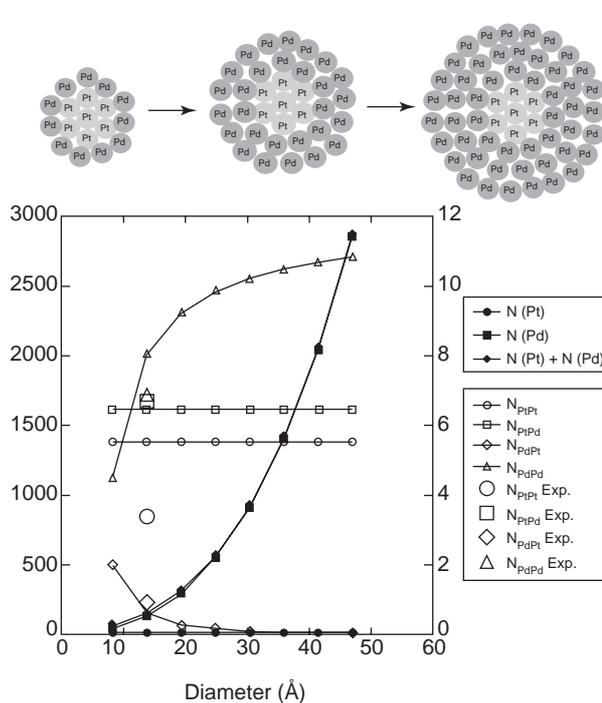
Coordination numbers N_{PtPt}, N_{PtPd}, N_{PdPt}, N_{PdPd} (the core of the cluster is composed of N(Pt) atoms Pt and surface is made of N(Pd) atoms Pd, the core of platinum atoms contains 13 atoms and the number of shells of palladium atoms is considered as a parameter) compared to experimental values.
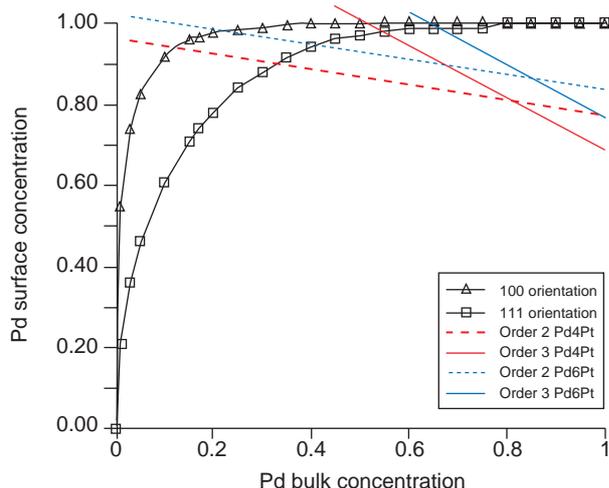
Figure 15

Theoretical predictions [23, 57] for the Pd surface segregation versus Pd bulk concentration of Pd_4Pt and Pd_6Pt catalysts. Surface composition of particles is obtained by the intersect of the curves 100 or 111 orientation and the straight lines.
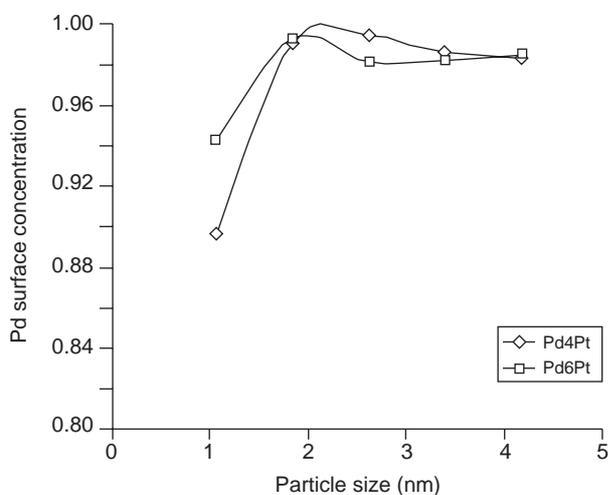

Figure 16

Pd surface compositions versus particle size calculated from the model described in references [23, 57].

The activity (7.2 h^{-1}) found for the Pd rich catalyst (Pd_6Pt) is slightly higher than one could expect considering the simple increase of exposed metallic surface area keeping the same particle size (6.6 h^{-1}).

One can assume that going from the Pd_4Pt to the Pd_6Pt, not only the number of active sites but also their intrinsic activity are increased. The Pd_6Pt catalyst has therefore an overall intrinsic activity in presence of sulfur higher than the Pd_4Pt catalyst.

Moreover, considering that more Pt atoms are accessible at the surface of the particles in the case of Pd_4Pt, and that the intrinsic activity of Pt is much higher than Pd (by a factor of 1.7), Pd_4Pt should be more active than Pd_6Pt without synergetic effect. Neither can a simple co-operative effect between Pd (hydrogen supplier) and Pt (aromatic hydorgenation site) as proposed in reference [23] explain our catalytic results.

Surface composition is clearly the key point for the understanding of the catalytic properties of bimetallic catalysts. Theoretical calculations as described in references [23, 56] allow the surface composition of small aggregates to be predicted. Application of this model to our case is presented on Figure 15. One can see that for cubooctahedron of order 2 (diameter of about 1 nm), the atomic surface composition of the Pd_4Pt is 90% palladium, the complement being platinum (10%), whereas in the case of Pt_6Pd these values are respectively 95% and 5%. On the basis of this theoretical calculation, we can say that more Pd atoms are accessible at the surface of the particles of the Pd_6Pt compared to the Pd_4Pt catalyst.

On Figure 16, are plotted, for the two bulk compositions, the evolution of Pd surface composition versus the particle size for a truncated cubooctahedron structure (order 2, 3, 4, 5 and 6). For particles smaller than 2 nm, the surface concentration decreases more quickly for the low Pd concentration Pd_4Pt than for Pd_6Pt. The bulk concentration in Pd_4Pt is not high enough to provide sufficient Pd atoms to have a full coverage of the surface of all the metallic particles. This point highlights the fact that the optimum bulk composition is size dependent and the Pd/Pt molar ratio of 4 often reported in literature as the best composition is appropriate in the case of large particles.

Keeping in mind that the real particle size distribution includes particles smaller than 1 nm, one can suppose that, in the case of the Pd_4Pt catalyst, a significant fraction of the overall metallic surface area corresponds to a Pd surface composition much lower than 100% with a significant fraction of exposed Pt atoms. The available amount of Pd, which tends to segregate, is lower than the number of surface sites and full coverage is not achieved. As was observed in a previous study [3], the optimum hydrogenation activity in presence of sulfur is obtained for a precise structure of the active site: a layer of Pd covering a Pt core with adsorbed sulfur coming from the testing conditions. This is not the case for the surface structure of Pt_4Pd and the better results for the Pd rich catalyst (Pd_6Pt) can be associated with this difference in terms of Pd surface composition.

The synergy between palladium and platinum can also be shown if we compare rate constants, determined for the starting feed containing 20 ppm sulfur, of pure Pd and Pt monometallics as shown on Table 5. Because rate constants of the bimetallic catalysts are both higher than those of pure monometallic catalysts, no additivity effect, whatever the size of the catalytic site, can account for this experimental result.

TABLE 5

Comparison of constant rate k (h^{-1}) for the starting feed (20 ppm S) for the monometallic and bimetallic catalysts

	pure Pd	**pure Pt**	**Pd$_4$Pt**	**Pd$_6$Pt**
k (h^{-1})^a	1.0	1.4	4.4	7.2
TON (h^{-1})	312	542	1405	1490

^{a} Constant rates are evaluated with a precision of 3%.

In addition, the sulphur/metal ratios measured on the used catalysts after hot washing with toluene and taking into account the sulphur adsorbed on the alumina carrier, are significantly lower for the bimetallic catalysts (0.1 and 0.2) than for monometallic Pt (0.5). This difference of amount of adsorbed sulphur between mono and bimetallic catalysts has also been observed in a previous study [3] and related to the core-shell structure. The Pd surrounding the Pt atoms inhibits the sulfidation of the Pt atoms, as shown by EXAFS measurements, where no Pt-S bonds in the bimetallic catalysts were observed.

CONCLUSION

In the work presented here, TEM, X-ray absorption spectroscopy and volumetric H_2-O_2 titration were used to characterize the structure and the composition of the metallic particles in bimetallic PdPt/Al$_2$O$_3$ catalysts for aromatic hydrogenation and desulphurization treatments.

Such a study is an important step to improve our understanding of catalytic phenomena at a nanometer scale and to establish structure – reactivity relationships. The results obtained by the different techniques give complementary information on both structure and composition of the metallic particles. Most of the particles are very small (less than 1 nm). In the majority, the particles were found bimetallic, with a "cherry" structure with a preferential distribution of palladium atoms at the cluster surface. It has been shown that the optimum Pd/Pt molar ratio is size dependent and must be adjusted in order to keep the precise bimetallic structure (core of Pt surrounded by a complete shell of Pd).

ACKNOWLEDGEMENT

REFERENCES

1 Official Journal of the European Union, 22.2.2003, Annex IV, L 76/19. In addition to their carcinogenic characteristic, mono- or poly-cyclic aromatics lowers the diesel fuel quality by lowering the cetane index.

2 Barbier, J., Lamy-Pitara, E., Marecot, P., Boitiaux, J.P., Cosyns, J., and Verna, F .(1990), *Adv. Catal.*, **37**, 279.

3 Guillon, E., Lynch, J., Uzio, D. and Didillon B. (2001), Characterization of bimetallic Pt systems: application to the reduction of aromatics in presence of sulfur, *Catalysis Today* **65**, 201.

4 Albertazzi S., Busca G., Finocchio E., Glöckler R. and Vaccari A. (2004), *J Catal* **223**, 272-381.

5 M Jacquin, DJ Jones, J Rozière, S Albertazzi, A Vaccari, M Lenarda, L Storaro and R Ganzerla (2003), *Applied Catal A*, **251**, 131.

6 Yasuda H., Matsubayahi N., Sato T. and Yoshimura Y. (1998), *Catal. Lett.*, **54**, 23.

7 Matsubayashi N., Yasuda H., Imamura M. and Yoshimura Y. (1998), *Catal. Today*, **45**, 375.

8 Rodriguez-Castellon E., Mérida J., Diaz L., Maireles-Torres P., Jones D.J., Rozière J. and Jimenez-Lopez A. (2004), *Applied Catal A*, **260**, 9.

9 Fujikawa T., Idei K., Ebihara T., Mizuguchi H. and Usui K. (2000), *Applied Catal. A*, **192**, 253.

10 Jongpatiwut T.S., Li Z., Resasco D.E., Alvarez W.E., Sughrue E.L. and Dodwell G.W. (2004), *Applied Catal. A*, **262**, 241-253.

11 Yasuda H., Sato T. and Yoshimura Y. (1999), *Catal. Today*, **50**, 63.

12 Pawelec B., Cano-Serrano E., Campos-Martin J.M., Navarro R.M., Thomas S. and Fierro JLG (2004), *Applied Catal. A*, **275**, 127-139.

13 US patent 6235915B.

14 Stanislaus S.A. and Cooper B.H. (1994), *Catal. Rev. Sci. Eng.,* **36**, 75.

15 Suchanek A.J. (1990), *Oil & Gas J.*, **7**, 109.

16 Kabe T., Qian W., Hirai Y., Li L. and Ishihara A. (2000) Hydrodesulfurization and Hydrogenation Reactions on Noble Metal Catalysts: I. Elucidation of the Behavior of sulfur on alumina-Supported Pt and Pd Using the 35S Radioisotope Tracer Method, *J. Catal.*, **190**, 191.

17 Jacquin M., Jones D.J., Roziere J., Lopez A.J., Rodriguez-Castellon E., Menayo J.M.T., Lenarda M., Storaro L., Vaccari A. and Albertazzi S. (2004), *J. Catal.*, **228 (2)**, 447-459.

18 Fujikawa T., Tsuji K., Mizugushi H., Godo H., Idei K. and Usui K. (1999), *Catal Lett.*, **63**, 27-33.

19 Toshima N., Harada M., Yonezawa T.,Kushihashi K. and Asakura K. (1991), Structural analysis of polymer-protected PdPt bimetallic clusters as dispersed catalysts by using Exafs, *J. Phys. Chem.,* **95**, 7448.

20 Kolb U., Quaiser S.A., Winter M. and Reetz, M.T. (1996), Investigation of Tetraalkylammonium Bromide Stabilized Pd/Pt bimetallic clusters using Exafs, *Chem. Mater.*, **8**, 1889.

21 Micheaud-Especel C., Bazin D., Guérin M., Marecot P. and Barbier J. (2000), Study of supported Pd-Pt catalysts. IR and Exafs characterisations and catalytic activity for toluene hydrogenation, *Reac. Kin. & Cat. Lett.*, **69**, 209.

22 Renouprez A., Rousset J.L., Cadrot A.M., Soldo Y. and Stievano L. (2001), Structure and catalytic activity of PdPt aggregates obtained by laser vaporisation of bulk alloys, *J. of Alloys and Compounds*, **328**, 50.

23 Rousset J.L., Stievano L., Cadete Santos Aires F.J., Geantet C., Renouprez A.J. and Pellarin M. (2001), Hydrogenation of toluene over γ-Al$_2$O$_3$ supported Pt, Pd and Pd-Pt model catalysts obtained by laser vaporization of bulk metals, *J. Catal.*, **197**, 335.

24 Rousset J.L., Stievano L., Cadete Santos Aires F.J., Geantet C., Renouprez A.J. and Pellarin M. (2001), *J. Catal.*, **202**, 163.

25 Wu M.L., Chen D.H. and Huang T.C. (2001), Preparation of Pd/Pt Bimetallic Nanoparticles in Water/AOT/Isooctane Microemulsions, *J. of Colloid and Interface Science*, **243**, 102.

26 Jan C.A., Lin T.B. and Chang J.R. (1996), *Ind. Eng. Chem. Res.*, **35**, 3893.

27 Bazin D., Triconnet A. and Moureaux P. (1995), An Exafs characterisation of the highly dispersed bimetallic PtPd catalytic system, *NIM B* 97, 41.

28 Le Bihan L. and Yoshimura Y. (2002), Control of hydrodesulfurization and hydrodearomatization properties over bimetallic Pd-Pt catalysts supported on Yb-modifed USY zeolite, *Fuel*, **81**, 491.

29 «Catalyst Characterization under Reaction Conditions», Topics in Catal. 8, 1/2 (1999) Ed. Gabor A. Somorjai, Sir J. M. Thomas., «EXAFS Spectroscopy in Catalysis», Ed. D.C. Koningsberger, B. L. Mojet, *Topics in Catal.* 10, 3/4 (2000).

30 Boitiaux J.P., Cosyns J., Vasudevan S. (1983), *Applied Catal. A*, **6** , 41.

31 Merlen E., Beccat P., Bertolini J.C., Delichère P., Zanier N. and Didillon B. (1996), *J. Catal.,* **159**, 178-188.

32 Van Hardeveld R. and Hartog F. (1969), *Surf. Sci.*, **15**, 189.

33 Singman C.N. (1984), *J. Chem. Ed.*, **61**, 137.

34 Bazin D., Dexpert H. and Lynch J. (1995), *In situ XAFS measurements of catalysts. Y. Iwasawa, Xas for catalyts and surfaces*, Ed., World Scientific.

35 Lynch J. (2002), Development of Structural Characterisation Tools for Catalysts. *Oil & Gas Science and Technology*, **57**, 281.

36 Sayers D.E. and Bunker B.A. (1998), *X-ray Absorption : Principles, Applications, Techniques of Exafs, Sexafs and Xanes*, D. C. Koningsberger, R Prins, eds, John Wiley & Sons Ed., 211.

37 Michalowicz A. and Vlaic G. (1998), Multiple solutions in data fitting: a trap in Exafs structural analysis and some ideas to avoid it, *J. Synch. Rad.*, **5**, 1317.

38 Khodakov A., Barbouth N., Oudar J., Villain F., Bazin D., Dexpert H. and Schulz, P. (1996), Investigation of dispersion and localisation of Pt species in mazzite using Exafs, *J. of Phys. Chem.*, **101**, 766.

39 Harada M., Asakura K. and Toshima N. (1994), Structural analysis of polymer-protected PtRh bimetallic clusters using Exafs. Importance of microclusters for the formation of bimetallic clusters, *J. of Phys. Chem.*, **98**, 2653.

40 Bazin D., Sayers D., Rehr J. and Mottet C. (1997), Numerical simulation of the Pt LIII edge white line relative to nanometer scale clusters, *J. of Phys. Chem.*, **101**, 5332.

41 Ankudinov A.L., Rehr J.J., Low J. and Bare S.R. (2001), Effect of Hydrogen Adsorption on the Xas of Small Pt Clusters, *Phys. Rev. Lett.*, **86**, 1642.

42 Bazin D. and Rehr J.J. (2003), Limits and advantages of X-ray absorption near edge structure for nanometer scale metallic clusters, *J. Phys. Chem. B*, **107**, 12398.

43 Bazin D., Sayers D. and Rehr J. (1997), Comparison between Xas, Awaxs, Asaxs & Dafs applied to nanometer scale metallic clusters, *J. Phys. Chem.*, **101**, 11040.

44 Yasuda H., Imamura M. and Yoshimura Y. (1998), Exafs study on PdPt catalyst supported on USY zeolite, *Catalysis Today*, **45**, 375.

45 Hansen P.L., Molenbroek A.M. and Ruban A.V. (1997), Alloy formation and surface segregation in zeolite-Supported Pt-Pd Bimetallic Catalysts. *J. Phys. Chem. B*, **101**, 1861.

46 Rades T., Pollisset-Thfoin M., Bonnin D., Bazin D. and Fraissard J., (1997), Segregation in a bimetallic Pd-Pt/NaY catalyst as seen by Exafs, *J. de Phys. C2*, 933.

47 Fujikawa T., Idei K., Ohki K., Mizuguchi H., and Usui K. (2001), Kinetic behavior of hydrogenation of aromatics in diesel fuel over silica-alumina-supported bimetallic PtPd catalyst, *Applied Catal. A : General*, **205**, 71.

48 Henry C. (1998), Surface studies of supported model catalysts, *Surf. Sci. Rep.*, **31**, 231.

49 Desjonqueres M.C. and Spanjaard D. (1995), *Concepts in surface physics*, Ed. Springer.

50 Bazin D., Mottet C., Treglia G. and Lynch J. (2000), New trends in heterogeneous catalysis processes on metallic clusters from synchrotron radiation and theoretical studies, *Applied Surf. Sci.*, **164**, 140.

51 Bazin D., Mottet C. and Treglia G., (2000), New opportunities to understand heterogeneous catalysis processes through synchrotron radiation studies and theoretical calculations of density of states : The case of nanometer scale bimetallic particles, *Applied Catal.: General A*, **200**, 47.

52 Fiermans L., De Gryse R., De Doncker G., Jacobs P.A. and Martens J.A. (2000), Pd Segregation to the Surface of Bimetallic PtPd Particles Supported on H- Zeolite Evidenced with XPS and Argon Cation Bombardment, *J. Catal.*, **193**, 108.

53 Yashima M., Falk L.K.L., Palmqvist A.E.C. and Holmberg K. (2003), Structure and catalytic properties of nanosized alumina supported Pt and Pd particles synthesized by reaction in microemulsion, *J. of Colloid and Interface Science*, **268**, 348.

54 Solla-Gullón J., Montiel V., Aldaz A. and Clavilier J. (2002), Electrochemical and electrocatalytic behaviour of PtPd nanoparticle alloys, *Electrochemistry Communications,* **4**, 716.

55 D'Souza L. and Sampath S. (2000), Preparation and characterization of silane-stabilized, highly uniform, nanobimetallic Pt-Pd Particles in Solid and Liquid Matrixes, *Langmuir,* **16**, 8510.

56 Rousset J.L., Bertolini J.C., Miegge P. (1996), *Phys. Rev. B*, **53**, 4947.

Final manuscript received in June 2005